Supplementary information to the manuscript: Word and bit line operation of a $1 \times 1\ \mu m^2$ superconducting vortex-based memory

SAMPLE FABRICATION

The studied devices were made from a single Nb (70 nm) film. It was deposited by the dc-magnetron sputtering at room temperature on an oxidized Si wafer. First, the film was patterned into $\sim 5\ \mu$m-wide bridges by photolithography and reactive ion etching. Subsequently, it was nano-patterned by Ga^+ focused ion beam (FIB). The readout junctions have a variable-thickness-bridge structure. They were made by cutting narrow grooves in the Nb film by FIB. The cuts are made as single-pixel lines with the nominal etching depth of typically 60 nm, using standard Si-milling parameters (volume-per-dose 0.27 μm^3/nC) at an ion current of 10 pA (30 keV). The etching time is calculated automatically for the chosen depth and volume-per-dose. The actual depth of the cut is, however, reduced by redeposition of Nb. The groove has a V-shape profile with the aspect ratio (depth/width) ~ 2. From the inset in Fig. 2 (a) it can be seen that the groove width at the surface is ($\sim 20 - 30$ nm), from which the actual depth can be estimated $\sim 40 - 60$ nm. Self-limiting of the cut depth is consistent with a slow increase of junction resistances with increasing the nominal depth. The vortex trap (a hole $\sim 50 - 100$ nm in diameter) is also made by FIB. All studied devices have a similar cross-like geometry, as can be seen from Fig. 2 (b). The four-terminal configuration allows both word and bit line operation and an independent measurement of the characteristics of both JJs.

CHARACTERISTICS OF 5 μm CELLS

Supplementary Figure 1 shows the current-voltage characteristics of cells with lengths $L_x \sim 5\ \mu$m. Fig. 1 (a) shows the temperature variation of I-Vs at zero field. In Fig. 1 (b) the I-Vs at four magnetic fields and a fixed T are shown. Typical resistively-shunted Josephson junctions behavior is observed. All studied JJs show similar characteristics.

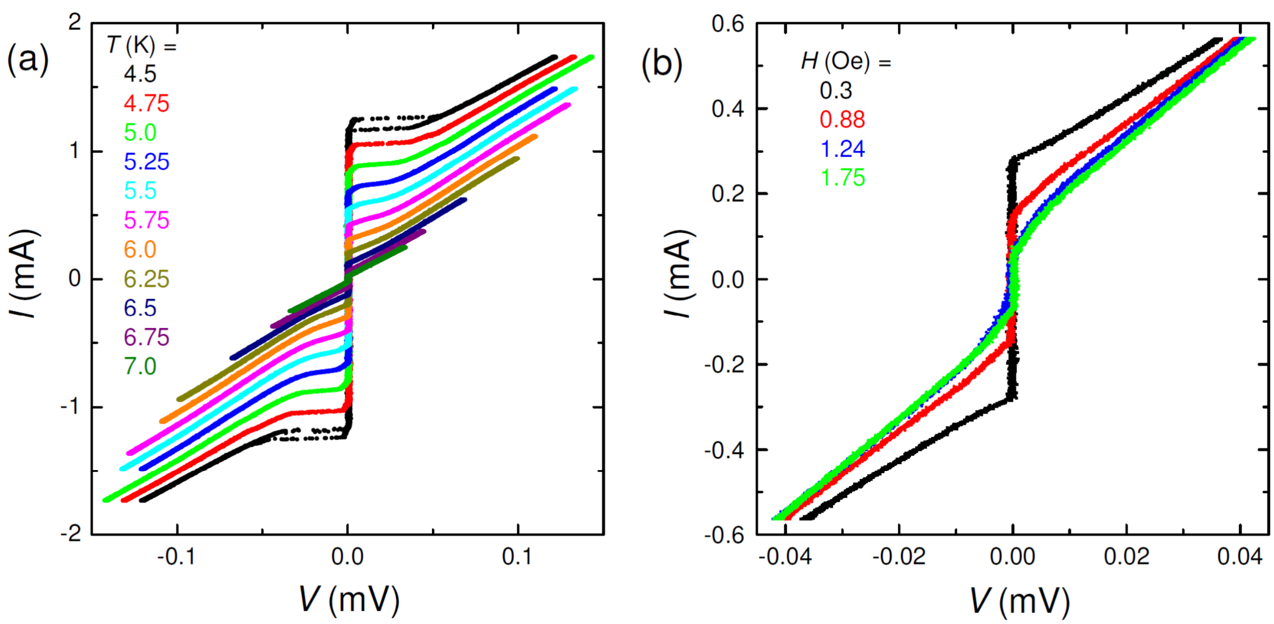

Supplementary Figure 1.
The current-Voltage characterisitics of Josephson junctions on two AVRAM cells with $L_x \sim 5\ \mu$m. (a) A set of I-V characteristics at different temperatures and $H \simeq 0$. (b) A set of I-Vs at four magnetic fields and $T = 6.65$ K (for another junction with a nominal depth of the groove 50 nm).

Supplementary Figure 2 (a) shows a SEM image of the largest cell with $L_x \simeq 5\ \mu$m on the same chip, as presented in the manuscript. Figs. 2 (b-c) shows measured $I_c(H)$ modulations for both JJs on this cell (b) without a vortex, (c) with a trapped vortex and (d) with a trapped antivortex.

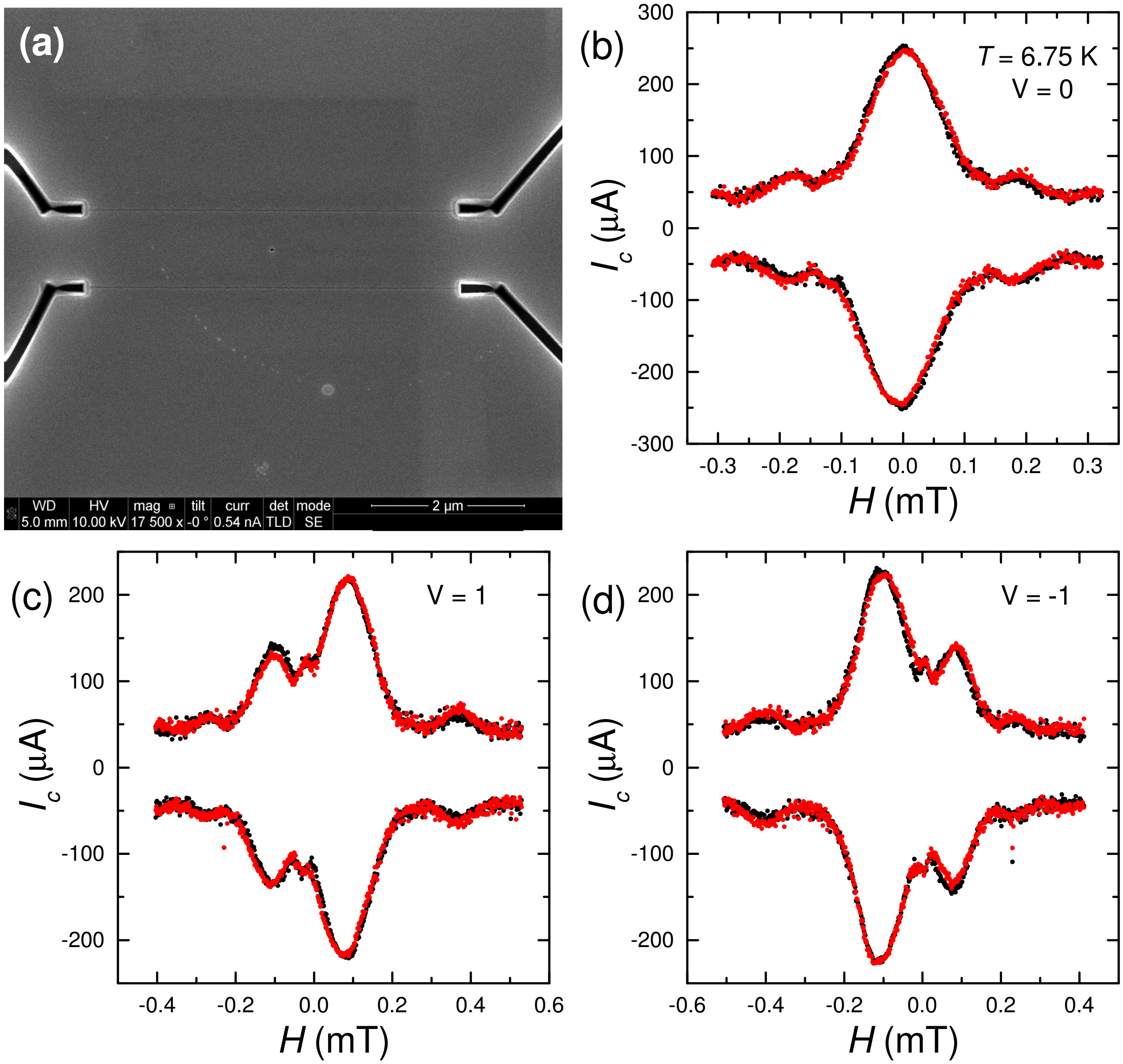

Supplementary Figure 2. **Chracteristics of a larger cell on the same chip.** (a) SEM image of the cell with $L_x = 5\ \mu$m on the same chip, as studied in the manuscript. (b-d) Measured $I_c(H)$ modulations for both JJs on this cell (black and red symbols): (b) without a trapped vortex, V=0; (c) with a trapped vortex, V=1; and (d) with an antivortex, V=-1. All measurements were performed at $T = 6.75$ K.

From the comparison of $I_c(H)$ patterns in Figs. 1 (c), (d) and Fig. S2 (b) it can be seen that the flux quantization field, ΔH, is increasing with decereasing junction length. $\Delta H = \Phi_0/A$, is determined by the effective flux quantization area, A. For our planar junctions with dissimilar electrodes (the outer electrode is very long and the inner is narrow) it is equal to $A = \left[L_x^2/1.8 + L_x L_z/2\right]/2$ [33]. Here L_z is the effective width of the inner electrode. Since this electrode is shared by both JJs, $2L_z = w$, where w is the separation between JJs, $w \simeq 1\ \mu$m. Thus,

$$\Delta H = 2\Phi_0 \left[\frac{L_x^2}{1.8} + \frac{L_x w_z}{4}\right]^{-1}.$$

This expression describes very well the observed flux-quantization fields.

TEST JUNCTION RESPONSE

The $1 \times 1\ \mu\mathrm{m}^2$ cell, analyzed in the maniscript contains two JJs. In the manuscript we showed only characteristics of the readout JJ near the vortex trap. The Supplementary Figure 3 shows simultaneously measured responses of both JJs on this cell for the case, corresponding to Fig. 3 (b). It is seen that the resistances of both JJs are correlated, but the response of the test junction is much smaller because of a significantly larger distance to the vortex trap.

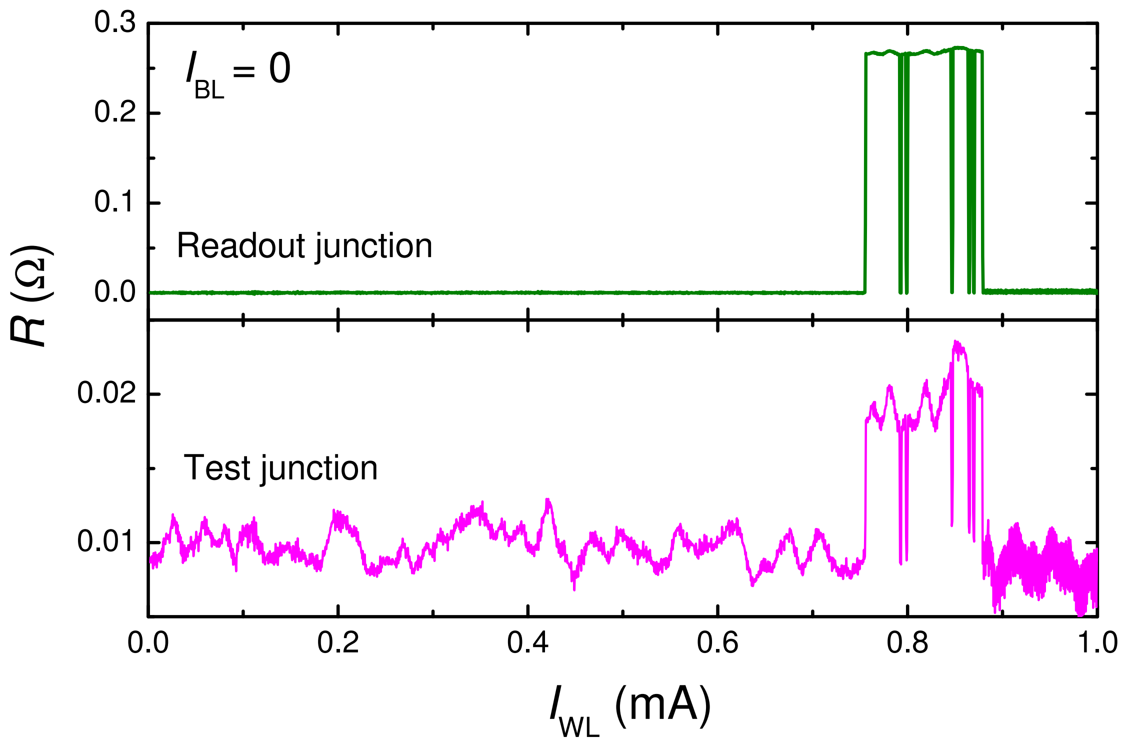

Supplementary Figure 3. **Demonstration of a test junction responce.** Simultaneously measured resitances of the readout JJ (top) and the test JJ (bottom) as a function of the wordline pulse amplitude for the case from Fig. 3 (b). A correlated responce of both junctions is seen, confirming that the vortex is indeed placed in the trap.

WORD AND BIT-LINE OPERATION

Supplementary Figure 4 demonstrates shapes of currents sent via wordline (a) and bitline (b) for the $1 \times 1\ \mu m^2$ cell. A single short pulse (in this case with the amplitude $+29\ \mu$A) is sent through the WL. The bit line current consists of the sinusoidal ac-current at a frequency $f = 23$ Hz and a short pulse (in this case with the amplitude $-230\ \mu$A), synchronized with the WL pulse. The BL current passes through the readout JJ, see Fig. 2 (a) and (b). The ac current is used for a continuous readout of the cell state via lock-in measurements of the junction resistance. The amplitude of the ac-current, $I_{ac} = 130\ \mu$A, is such that it is larger than $I_c(\mathrm{V} = \pm 1) \simeq 100\ \mu$A, but smaller than $I_c(\mathrm{V} = 0) \simeq 150\ \mu$A, see Fig. 3 (a). Therefore, the V=0 state has zero resistance and V=±1 states have finite resistances, $R \sim 0.3\ \Omega$, as shown in Fig. S3. Rightmost panels represent closeups on the pulse sequencies. It can be seen that the BL pulse is applied at zero of the ac-current. The switching occurs very rapidly at the time scale much shorter than the period of the ac-current ~ 43 ms. Therefore, the ac current does not interfere with the pulses and does not affect the switching. The programed pulse widths are about 17 μs. The rightmost panels represent actual measurements of the flowing currents. They are broadened by the time delays in the twisted pairs through which the current pulses are delivered to the sample and the response voltage is transmitted back to the measurement equipment.

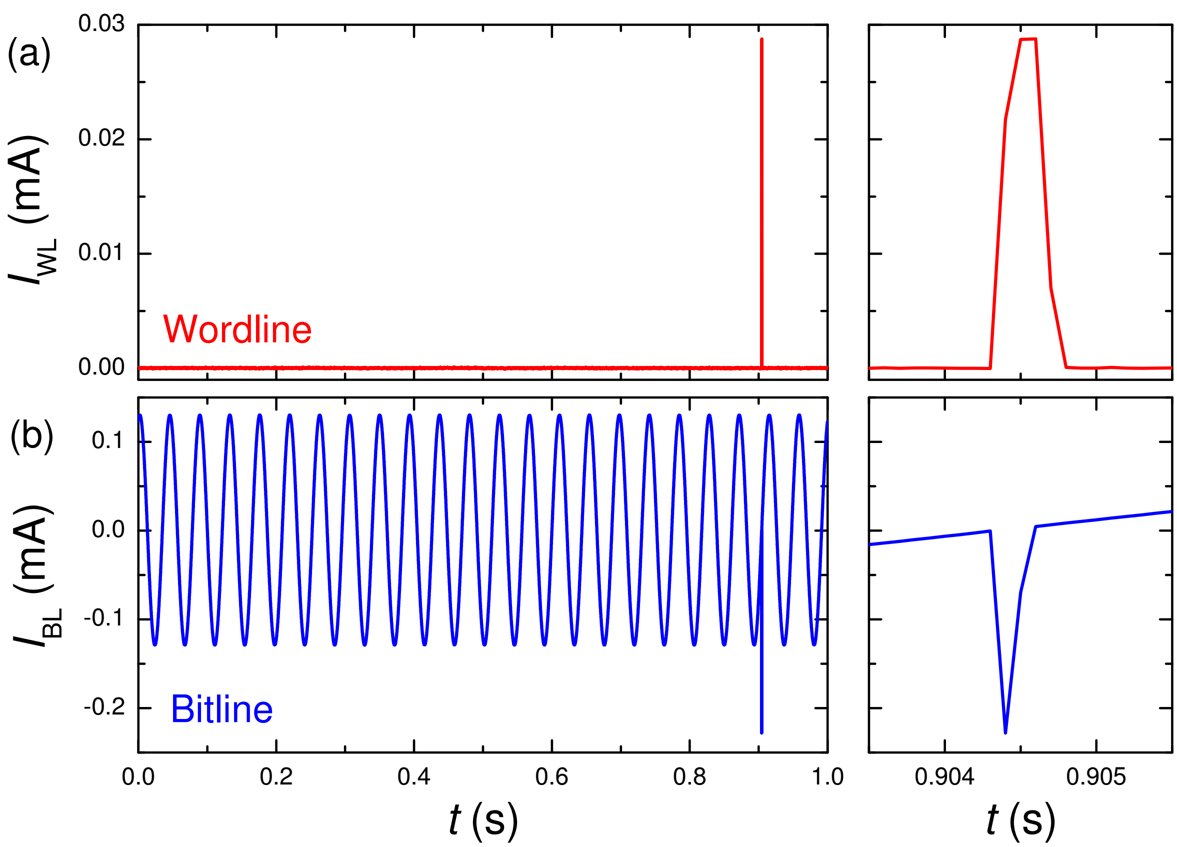

Supplementary Figure 4. **The shapes of pulses sent via word and bit lines in the $1 \times 1\ \mu m^2$ cell.** Panels (a) and (b) show measured time-dependencies of currents flowing through the wordline (a) and bitline (b). The WL contains a single puls. The BL current is a combination of a sinusoidal current at $f = 23$ Hz, which is used for the continuous readout of the junction resistance and a sharp pulse, synchronized with the pulse in the WL. Rightmost panels show enlarged views of the two pulses.

Supplementary Figure 5 illustrates the write operation at $I_{\mathrm{BL}} = \pm 0.37$ mA versus I_{WL} of both signs. It can be seen that the switching process is centrosymmetric: $I_{\mathrm{WL}}(I_{\mathrm{BL}}) = -I_{\mathrm{WL}}(-I_{\mathrm{BL}})$. However, the vorticity has opposite signs in the centrosymmetric states, as indicated in the Figure. Such behavior is expected if vortices are following the same route (the easy track) under the influence of Lorentz forces from both currents.

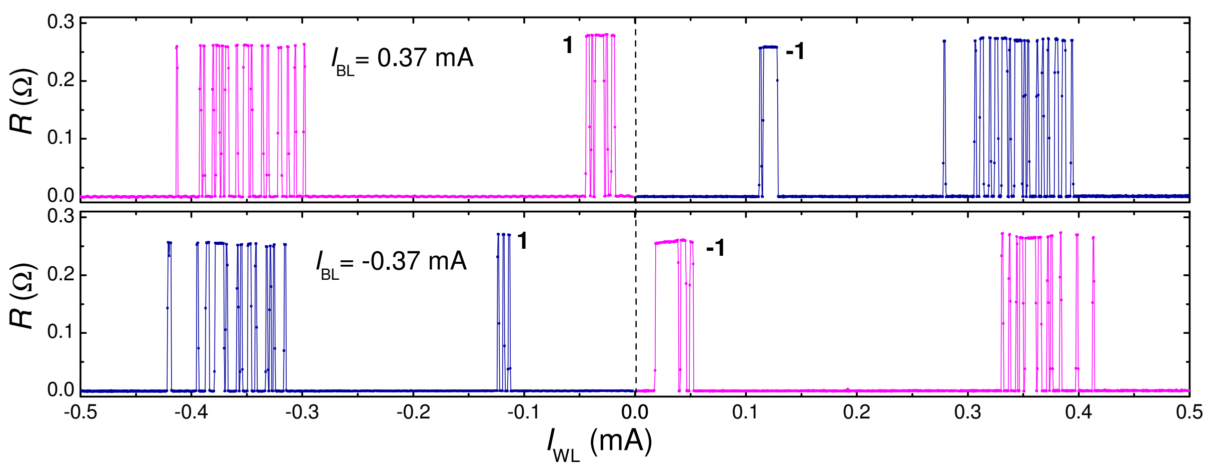

Supplementary Figure 5. Word and bit-line operation of the 1×1 μm^2 cell. The readout junction resistance is shown as a function of the WL pulse amplitude, I_{WL}, for fixed amplitudes of the BL current. $I_{\mathrm{BL}} = \pm 370$ μA and I_{WL} of either directions. The color emphasizes the centrosymmetric response, $R(I_{\mathrm{WL}}, I_{\mathrm{BL}}) = R(-I_{\mathrm{WL}}, -I_{\mathrm{BL}})$, accompanied by the flipping of the vortex sign ($\pm 1 \rightarrow \mp 1$).

HIGH-ENDURANCE OPERATION

Supplementary Figure 5 demonstrates high-endurance operation of the $1 \times 1\ \mu\mathrm{m}^2$ cell for sequencies of WL pulses from Figs. 4 (b) and (c).

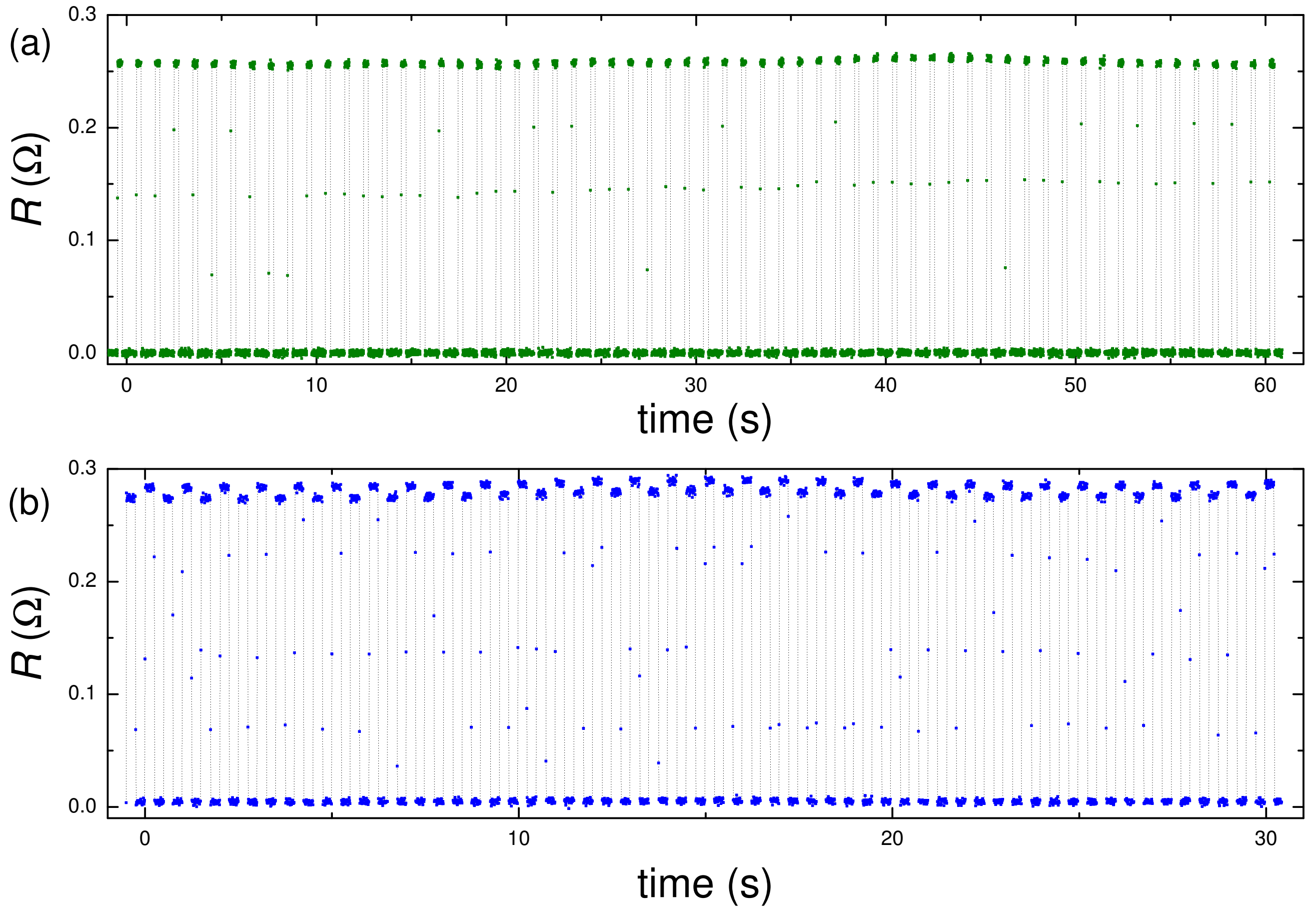

Supplementary Figure 6. **Demonstration of high-endurance operation of the $1 \times 1\ \mu\mathrm{m}^2$ cell.** Extended time dependence of the readout junction resistance for the following operations: (a) $0 \rightarrow -1$ switching for a WL pulse train from Fig. 4 (b); and (b) $0 \rightarrow -1 \rightarrow 0 \rightarrow 1$ switching for a WL pulse train from Fig. 4 (c).